New Plasma Tools for Antimatter Science

J. R. Danielson, T. R. Weber and C. M. Surko

Department of Physics, University of California, San Diego La Jolla CA 92093

Abstract. Recent research is described that exploits nonneutral plasma techniques to develop new tools to accumulate, manipulate and store antimatter and to make cold, bright antiparticle beams. Progress is described in three areas: radial compression of single-component plasmas using rotating electric fields in a novel, strong-drive regime; experiments and complementary theoretical modeling of the extraction of antiparticle beams with small transverse spatial extent from single-component plasmas; and work to develop a multicell trap to increase, by orders of magnitude, the capacity for antiparticle storage. Potential applications of these tools and challenges for future research are discussed.

Keywords: antimatter, positrons, cold plasmas, low-emittance beams
PACS: 52.55Dy, 52.27.-h, 52.27Aj, 52.25Fi

I. INTRODUCTION

Much progress has been made recently to create cold antimatter plasmas and to exploit them for a variety of fundamental scientific studies and technological applications [1]. A key focus of this conference has been efforts to create, trap, and study antihydrogen [2-5]. Other examples that require positrons are studies of electron-positron plasmas [6-8], positron interactions with atoms and molecules [9, 10], modeling of astrophysical processes [11, 12], and the characterization of materials [13, 14]. On the horizon, a new generation of more intense positron sources is under development [15-18]. Full utilization of these facilities will require new plasma techniques for a range of applications including study of the positronium molecule, Ps_2 [19, 20], the formation of BEC gasses of positronium atoms [21, 22], and the study of electron-positron plasmas [8, 23].

We describe here recent research to develop new tools to create and manipulate single-component plasmas. Electron plasmas (used for convenience and high data rate) are compressed radially using rotating electric fields [the so-called "rotating wall" (RW) technique]. The work focuses on a regime in which the plasma spins up until the plasma rotation frequency is equal to the applied frequency [24]. This creates a rigidly rotating plasma with a known and constant high density. Studies are also described to extract beams of small transverse spatial extent from the plasma center [25, 26]. The factors determining the radial beam profile and minimum beam width are identified. Finally, work is described to develop a multicell trap capable of storing orders of magnitude more positrons than is currently possible (e.g., particle numbers, $N > 10^{12}$) [27, 28].

CP1037, *Cold Antimatter Plasmas and Application to Fundamental Physics*, edited by Y. Kanai and Y. Yamazaki

II. DESCRIPTION OF THE EXPERIMENTS

Plasmas were confined in a Penning-Malmberg trap shown schematically in Fig. 1 and described in detail in Ref. [29]. It consists of a series of room-temperature, cylindrical electrodes 0.5 m in total length with inner radii, R_W = 1.27 cm. A uniform magnetic field, B = 4.8 Tesla, is imposed parallel to the electrode axis. In equilibrium, the plasma has a constant density profile with density n_0 (i.e., a "flat top" radial distribution), and undergoes E x B rotation at a frequency, $f_E = n_0 ce/B$ [18, 19]. The plasma temperature, $T \sim 0.05 - 0.1$ eV, which is uniform across the plasma, is set by the balance between heating sources (due to background drag and/or rotating wall torques) and cyclotron cooling (τ_C = 0.16 s) [18, 19].

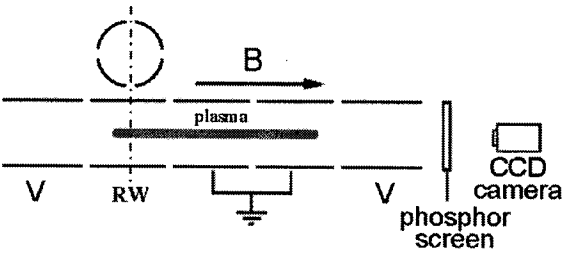

FIGURE 1. Schematic diagram of the Penning-Malmberg trap with segmented rotating wall electrode, phosphor screen and CCD camera.

Radial areal plasma density profiles are measured by releasing the trapped plasma, then accelerating the particles into a phosphor screen where the resulting light is imaged using a CCD camera. The plasma temperature is varied by repeated compression and expansion of the plasma (i.e., changing the plasma length), thereby heating the plasma through Coulomb collisions. The temperature, T, is determined by time-resolved measurement of the number of electrons escaping from the trap when the confining potential, V_C, at one end is slowly lowered [30].

III. ROTATING-WALL COMPRESSION IN THE STRONG DRIVE REGIME

The "rotating wall" (RW) technique, whereby a single-component plasma is compressed radially using a rotating electric field, has proven to be an important tool for antimatter research. This technique was first developed to tailor electron and ion plasmas [31, 32]. More recently, it has become a key tool to manipulate and tailor antimatter plasmas [33, 34]. In the work described here, phased sine waves applied to a sectored electrode are used to generate a rotating electric field with azimuthal mode number, $m_\theta = 1$ [24, 29]. These fields produce a torque on the plasma, thereby compressing the plasma radially in a non-destructive manner. Early experiments achieved good coupling by matching the drive frequency, f_{RW} to Trivelpiece-Gould modes in the plasma [31]. However, this approach has the drawback that compression

is only possible at selected frequencies, and careful tuning of the drive frequency to the plasma modes (which change with plasma compression) is required.

We discovered two regimes in which such tuning is unnecessary, first in a positron plasma with buffer-gas cooling when the plasma radius is comparable to the Debye length, λ_D [33], and later in electron plasmas in a high-magnetic-field trap when the drive amplitude is sufficiently large [29]. Shown in Fig. 2 is an example of this later, "strong drive" regime. Above a certain drive amplitude (V_{RW} = 0.7 V p-p in the experiment shown in Fig. 2), the plasma evolves to a high-density steady state in which $f_E \approx f_{RW}$. The protocol for these experiments is such that an initial plasma is created and allowed to come to equilibrium, *then the RW is applied at fixed values of both V_{RW} and f_{RW}*. As illustrated in Fig. 3, the radial density profiles of these plasmas are "flat-top" in shape. Thus the plasma rotates rigidly at frequency f_E and is in an approximate thermal equilibrium state. Experiments at various values of f_{RW} are shown in Fig. 4, illustrating the ability to access a broad range of high-density states in this strong-drive regime.

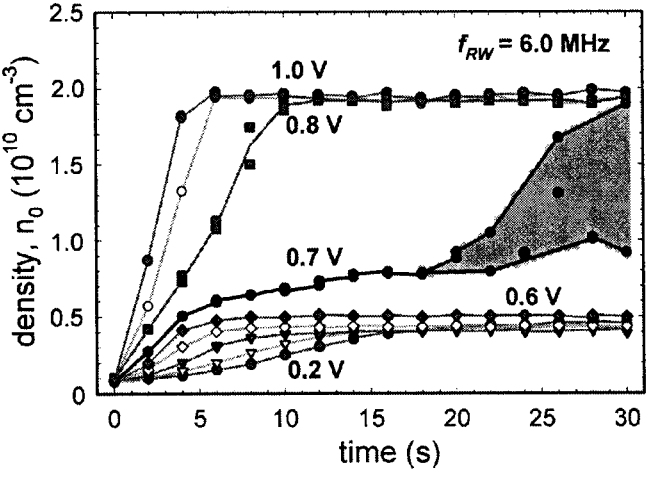

FIGURE 2. Central electron density is shown as a function of time for various amplitudes of applied RW voltage at 6 MHz. Note the bifurcation from a low-density to a high density state as V_{RW} is increased above 0.7 V. Reprinted from Ref. [29].

The central physics question that we addressed recently is what factors determine the ability to access this regime. The key insight came from examining closely behavior such as that illustrated in Fig. 4 (right), where a "step" appears in the data near some characteristic density, in this case $n_0 = 0.4 \times 10^{10}$ cm^{-3}. Close examination indicates that this corresponds to the situation in which a static asymmetry in the laboratory frame drives a Trivelpiece-Gould mode traveling backwards on the rotating plasma. In this case, the mode frequency is zero in the lab frame and referred to as a "zero frequency mode" (ZFM). Coupling of the static asymmetry to this mode causes a drag on the plasma creating an impediment to further compression [29].

In collaboration with T. M. O'Neil, we modeled the drag and drive torques on the plasma to include this ZFM-induce drag, namely [35],

$$\tau = \eta \frac{f_{RW} - f_E}{f_E} V_{RW}^2 - \frac{\beta f_E}{D^2 + f_E^2} - \frac{\gamma \delta f_0}{\left(f_E - f_0\right)^2 + \left(\delta f_0\right)^2}, \qquad (4)$$

where η, β, γ, and D are constants. The three terms in Eq. (4) represent, respectively, the RW drive, the background drag on the plasma due to trap imperfections, and the drag due to the ZFM. The form of the second term was chosen empirically to model the observed outward transport, and the ZFM is modeled by a Lorentzian of width δf_0, *centered* at frequency f_0.

The predictions of this model for the drive and drag torques are shown in Fig. 5. The plot on the left compares the RW drive torque, for a fixed frequency at various amplitudes, to the sum of the two drag torques from Eq. (4). At the locations where the drive and drag torques match, there is the possibility of a torque-balanced steady state (i.e., an attracting fixed point in the language of nonlinear dynamics). These steady states are shown in the right panel of Fig. 5. Due to the presence of the ZFM torque, there exist two stable steady states (closed circles) – one at high density and one at lower density – and an unstable state (open circles). Which stable state the plasma relaxes to depends on which side of the ZFM the plasma starts. As a consequence, the plasma is predicted to exhibit hysteresis as a function of the RW drive amplitude. Similar hysteresis is also predicted as a function of f_{RW} [35]. The key point is that the ZFM drag has the effect of inhibiting access to the high-density fixed point of the system until a sufficiently large value of V_{RW} is applied. Once in this high-density state, V_{RW} can be reduced significantly without producing much of a decrease

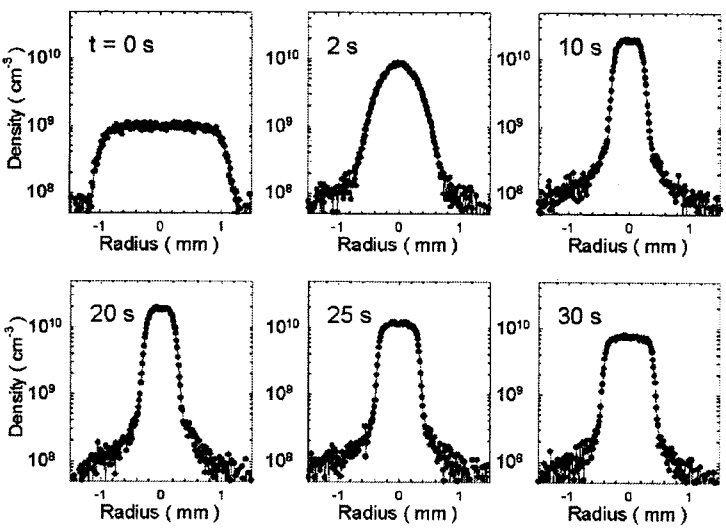

FIGURE 3. Radial profiles obtained by compression at 6 MHz beginning with the plasma at $t = 0$ s. The plasma is in steady-state compression from 10 to 20 s, then allowed to expand with the RW off. All profiles are close to thermal equilibrium with flat-top profiles, except at $t = 2$ s, where the plasma is much hotter, namely $T \sim 3$ eV. This data is reprinted from Ref. [29], where the experiment is described in more detail.

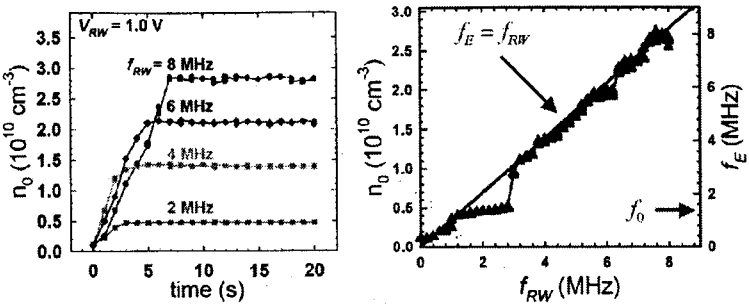

FIGURE 4. (left) central plasma density following application of the RW at various frequencies at V_{RW} = 1.0 V; and (right) steady-state density following the transition to the high-density state as a function of applied RW frequency. The step near n_0 = 0.5 x 10^{10} cm^{-3} is due to a so-called "zero-frequency" mode, which was key to understanding the bifurcation from low- to high-density steady states. Data from Ref. [29].

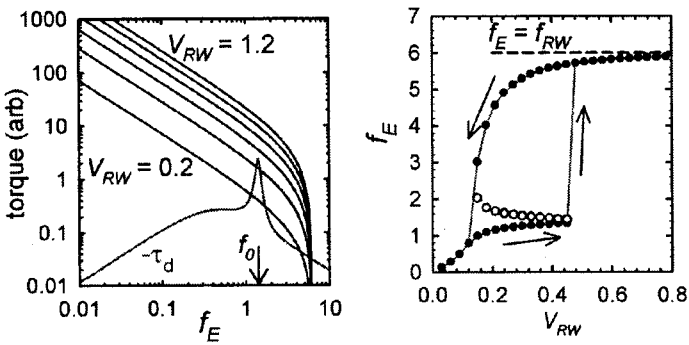

FIGURE 5. (left) the drag and drive torque from Eq. (1), shown at various drive amplitudes, V_{RW}; (right) the resulting torque-balanced steady states, illustrating the hysteretic behavior as a function of V_{RW}. All quantities are in arbitrary units. The predictions of the model are qualitatively in good agreement with the experimental results. This analysis is from Ref. [35]; see this reference for details.

in plasma density (i.e., the system exhibits considerable hysteresis). These predictions are in qualitative agreement with the experimental results, as is a similar hysteresis observed when f_{RW} is varied.

These results provide a physical model of access to the strong-drive regime and the high-density steady states that are achieved. We have made quantitative measurements of the RW torque on the plasma in the high-density state, with the hope that this will motivate a theory of torque in this state. The fact that the initial, final, and intermediate states are all close to thermal equilibrium provides reason to believe that a theory of the compression process might be possible. While admittedly speculative, the plasma evolution might be described, for example, as a series of thermodynamic equilibrium states with the rate-limiting process determined by one variable, such as the momentum relaxation time.

A key practical question now is what limits the compression and the maximum achievable density. Presently we do not know the answer. We are able to work with relative ease up to 8 or 9 MHz and, with some care, we have achieved states up to ~ 18 MHz. However, above 8 MHz, there are imbalances in the four legs of the RW drive

circuit likely due to (extrinsic) resonances in the cables and electrodes. This is curable. On the other hand, a generic model of the RW drive predicts that the electric fields due to the RW are screened in the Debye sheath at the plasma edge by particles moving along magnetic field lines. For an electrode of length L, the time to screen such a field (and hence develop a density perturbation upon which the RW electric field acts to produce a torque) is of order $L/2\bar{v}$, where $\bar{v}$ is the thermal particle velocity. As a result, frequencies $f_{RW} \geq \bar{v}/\pi L$ would be expected to be less effective in driving the required torque. Whether this is a practical limitation awaits further study.

IV. EXTRACTION OF BEAMS WITH SMALL TRANSVERSE SPATIAL EXTENT

Specially tailored particle beams have historically found a wealth of applications in science and technology, and this is proving especially true in studies involving antimatter [1]. Applications include the formation of antihydrogen, study of electron-positron plasmas, the formation of Ps_2 and BEC Ps, the use of positrons to characterize materials, and study of the interaction of positrons and Ps atoms with ordinary matter. For applications in which spatial resolution and/or high-quality beam emittance are required, beams with a small energy spread and small transverse spatial extent are desirable. For a single-component plasma in a Penning-Malmberg trap, the space charge potential is largest on the axis of the plasma. Recently, we exploited this fact to create beams of small transverse spatial extent by carefully lowering, in a pulsed manner, one of the confining end-gate potentials, V_C [25, 26].

A schematic diagram of the experimental arrangement is shown in Fig. 6. Of interest is the radial profile of the extracted beam, and in particular, the possible minimum beam diameter and the maximum number of particles that can be extracted in a pulse at this diameter. The potential, V_C, was lowered to carefully predetermined values by applying a 10 μs square-wave pulse with amplitude ΔV. The particles were found to escape in a time ~ 5 μs. Shown in Fig. 7 is an example of the areal plasma

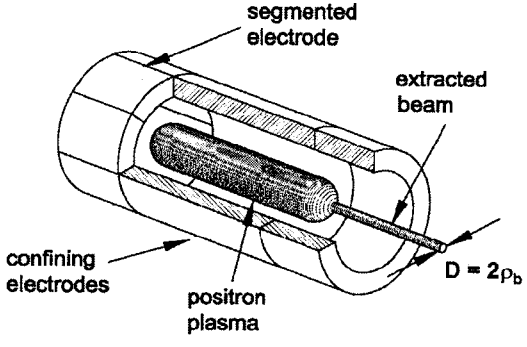

FIGURE 6. Experimental arrangement used to extract beams of small spatial extent from a single-component plasma by slowly lowering an end-gate potential in a Penning-Malmberg trap. The focus of the research described here is determining the minimum beam radius, ρ_b.

density profile before and after beam extraction and examples of radial profiles, $\sigma_b(r)$, for various extracted beams.

The results were analyzed by two methods. For the smallest-amplitude beams, we developed a simple analytic expression predicting Gaussian areal density profiles with a radius to 1/e of $\rho_b = 2\lambda_D$. For larger beams the expression for the width becomes [26]

$$\rho_b = 2\lambda_D\left[1+\xi\right]^{1/2}, \tag{2}$$

where

$$\xi = \frac{N_b}{N_0}\left(\frac{rp}{2\lambda D}\right)^2 = \frac{e\Delta\phi}{T} \tag{3}$$

is the critical parameter determining the growth of ρ_b with the amplitude of the extracted beam, with N_b/N_0 the fraction of the plasma extracted per pulse, and r_p is the plasma radius. As indicated in Eq. (3), $\xi = e\Delta\phi/T$, which is the ratio of the difference in space-charge potential across the beam, $\Delta\phi$, due to the N_b particles to the plasma temperature.

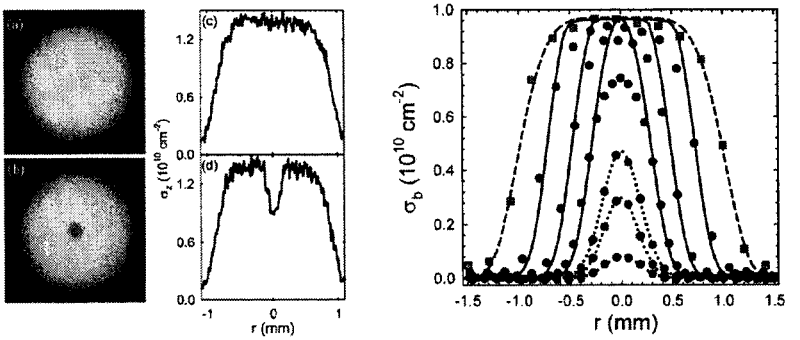

FIGURE 7. (left) CCD camera images of the areal density profiles (a) before; and (b) 10 μs after beam extraction, and in (c) and (d) the corresponding radial profiles, $\sigma_z(r)$; (right) profiles, $\sigma_b(r)$, of extracted beams for $\xi \approx 0.1, 0.3, 0.5, 1.0, 1.9, 2.8$. Shown for the three smallest beams are Gaussian fits (···), while the three largest beams are fit (–) to numerical solutions. The initial plasma profile, $\sigma_z(r)$, is also shown (■). Reprinted from Ref. [26].

When the factor $\xi \geq 0.5$, the profiles depart from the Gaussian predictions. In this case, the profiles were calculated numerically with the assumption that particles exit the plasma before scattering or radial diffusion occurs. As shown in Fig. 7, the profiles of small-amplitude beams fit well with the Gaussian predictions, and the profiles of larger amplitude beams are in reasonable agreement with the numerical calculations. As shown in Fig. 8, the predicted *beam widths* from Eqs. (2) and (3) are in good agreement with the data over the wide range of beam amplitudes studied.

A key result of these studies is that the beam diameter is limited to be $\geq 4\lambda_D$. Another important result is the identification of ξ as the parameter determining beam

widths. Equations (2) and (3) set a limit on the fraction of beam particles that can be extracted at the minimum diameter of $4\lambda_D$. Physically, this is the condition that the areal density within the pulse must be smaller than the areal density of the parent plasma, namely $(N_b/2\lambda_D)^2 < N_0/(r_p)^2$. Equations (2) and (3) also quantify the beam widths for larger beam pulses.

In practical applications, one would like to convert a trapped plasma into a train of approximately identical pulses. Shown in Fig. 9 is an example where over 50% of a trapped plasma was converted to a train of 20 nearly identical pulses. This was

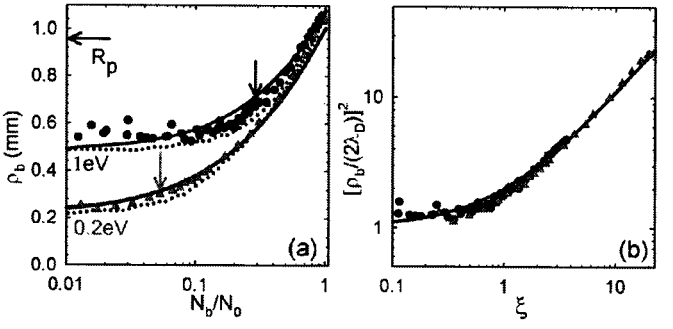

FIGURE 8. (a) Beam-width parameter, ρ_b, plotted vs. N_b/N_0 for T = 1.0 eV (●), and 0.2 eV (▲). Predictions (–) from Eqs. (2) and (3) with no fitted parameters, and (···) a numerical calculation from [26]. Arrows correspond to beams with ξ = 1. (b) Data from (a) plotted as $(\rho_b/2\lambda_D)^2$, vs. ξ, demonstrating the scaling predicted by Eqs. (2) and (3). Reprinted from Ref. [26].

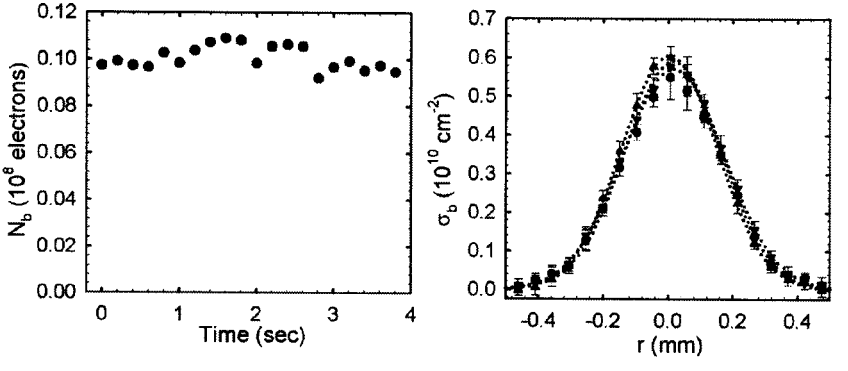

FIGURE 9. (left) Amplitudes, N_b, for 20 pulses extracted consecutively with $\langle N_b \rangle$ = 0.1 ± 0.005 x 10^8. $\xi \approx 0.2$. (right) areal density profiles for the 1st (●), 10th (▲), and 20th (▼) extracted beams. $N_b \approx$ 0.1 x 10^8 for all beams. The beam width remains approximately constant, λ_D is maintained invariant during the extractions; Gaussian fits to the profiles are also shown. Reprinted from Ref. [26].

accomplished by maintaining the central plasma density constant throughout the extraction process using the RW. After the extraction, the "holes" left by the extracted pulses propagate coherently to the plasma edge in a time < 1 ms. This returns the

plasma to a rigid rotor, thermal equilibrium state that would, in principle, allow pulse extractions at a kilohertz rate. Whether this is possible, given the fact that the plasma must be compressed with the RW to maintain constant *n and* λ_D, is an important topic for future research.

There are a number of potential applications of this technique. For example, there are situations in which an *electrostatic* as opposed to a magnetically guided beam is desirable. While the latter is most compatible with accumulation and storage in a Penning-Malmberg trap, the former admits to the use of electrostatic focusing and exploitation of ballistic trajectories in three dimensions. In Ref. [26], we provide an example of extracting a cold beam ($T \sim 10$ meV) from a plasma in a 5 tesla field. Assuming it is guided to a region where $B \sim 5$ gauss (i.e., 5×10^{-4} T) and then extracted from the field, this produces an electrostatic beam with a diameter of 1 mm and an energy spread of 10 meV (essentially all in the parallel direction). Such a beam would be a considerable advance for positron-atomic physics scattering experiments, and could potentially be used to form microbeams for materials analysis. For example, typical electrostatic beams used for atomic physics studies have energy spreads ≥ 200 meV and transverse extents ≥ 5 mm. Given the constraint on ξ (i.e., $\xi < 1$), the maximum number of particles per pulse for the 10 meV beam described here is $N_b \sim 4 \times 10^3$.

V. PROGRESS TOWARDS A MULTICELL TRAP

For a number of applications, one would like very large quantities of positrons – amounts that exceed the capabilities of current accumulation and storage techniques. In particular, typical cylindrical plasmas in Penning-Malmberg traps are space-charge limited at $\sim 10^9 \tilde{V}_C$ particles per centimeter of plasma length, where $\tilde{V}_C$ is the confining potential in kV [27]. Examples of potential applications requiring such large numbers of positrons include the study of electron-positron plasmas and the creation of a Bose-condensed gas of positronium atoms. Currently, new intense sources of positrons are planned or coming online at several laboratories throughout the world, and the ability to accumulate, cool and manipulate large amounts of positron plasma would facilitate efficient multiplexing of end-user experiments at these facilities.

We have begun development of a multicell Penning-Malmberg trap that circumvents this space-charge limit by arranging multiple Penning-Malmberg-trapped plasmas ("cells") in the same vacuum system and magnetic field, with these plasmas shielded from each other by copper electrodes [27, 28]. A schematic diagram of this trap is shown in Fig. 10. Positrons would first be accumulated using a buffer-gas trap, then transferred to a high-field trap (e.g., $B \sim 5 - 10$ T), where they would be cooled by cyclotron radiation in UHV. We propose to build a 100 cell trap with $\tilde{V}c \sim 1 - 2$ kV which would accommodate $N > 10^{12}$ positrons in ~ 100 cells. A convenient arrangement is 5 banks of 19 cells in the direction perpendicular to $B \sim 5$ T.

Recently, we have made considerable progress in establishing the technical basis for such a trap [26]. The confinement of $N > 10^{10}$ electrons in a plasma 10 cm in length with $\tilde{V}c = 1$ kV was demonstrated. The ability to operate two in-line cells simultaneously was also established. In addition, the multicell trap requires that a method be developed to move plasma efficiently across the magnetic field to fill off-axis cells with plasmas from the buffer-gas trap. This was accomplished using

autoresonant excitation of the diocotron mode, wherein a plasma at the center of a cylindrical electrode is driven off axis by a frequency-swept signal applied to a segmented electrode. The plasma phase-locks to the drive signal, and so it can be deposited at a precise radial and azimuthal location (i.e., required to fill off-axis cells in a multicell trap). Data demonstrating this capability are shown in Fig. 11. Positioning accuracy is ~ ± 0.1 mm, and it was demonstrated that plasmas can be

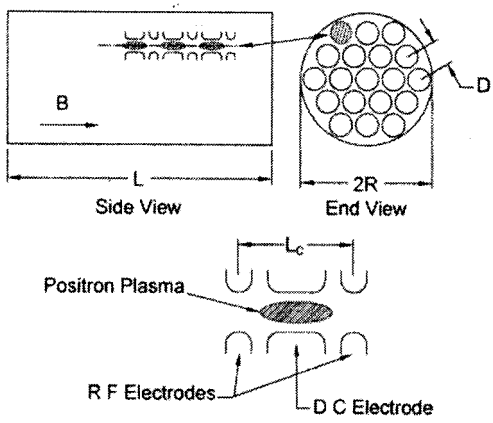

FIGURE 10. Conceptual design of a 95-cell trap showing the arrangement of cells parallel and perpendicular to B. The device consists of 19, hexagonally close-packed cells perpendicular to B and 5 in-line cells in the field direction.

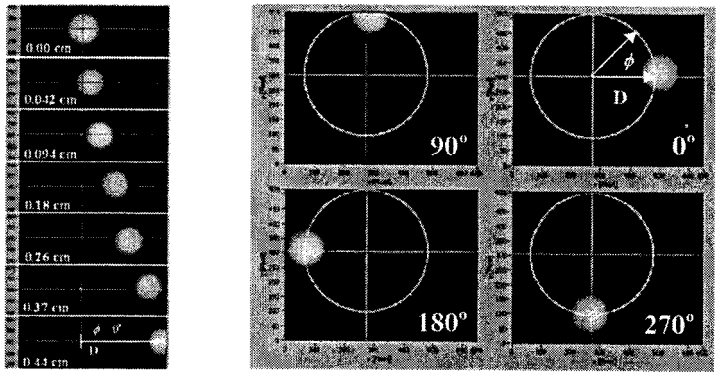

FIGURE 11. CCD camera images of displaced plasmas dumped on the phosphor screen using autoresonant, diocotron-mode excitation. (a) radial displacements at fixed azimuthal position; (b) azimuthal displacements at fixed radial position. From Ref. [28].

translated radially out to 80% of the electrode inner diameter. A schematic diagram showing the master cell for acceptance of plasmas from the buffer-gas trap and translation off axis and two banks of 19 storage cells is illustrated in Fig. 12.

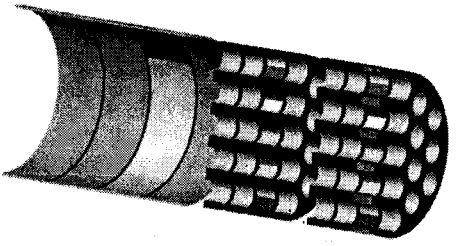

FIGURE 12. Cutaway view of the electrode structure design for a multicell trap: Large diameter electrodes form the master plasma-manipulation cell to receive plasmas from a buffer-gas trap and to displace them for deposition into off-axis cells. Also shown are two banks of 19 cells (38 cells total). In a 95 cell trap, there would be three more 19-cell banks at the right. From Ref. [28].

One remaining issue to be addressed is establishing that plasmas can be well confined (i.e., using RW compression to mitigate outward transport) in cells a significant distance off-axis and in regions of only modest magnetic field homogeneity (e.g., near the ends of the solenoid that provides the axial magnetic field). Experiments of this type are planned. We also plan experiments to establish the minimum electrode diameters that will be required for good confinement. This latter consideration will determine how compact such a device can be. Ultimately, one would like to have portable antimatter traps, but this will likely require advances in magnet technology to avoid the necessity of cryogenic cooling of the high-field magnet.

VI. CONCLUDING REMARKS

In this paper, we have summarized recent work on the development of nonneutral plasma-physics tools for antimatter studies. We have also highlighted important issues for future research. In the area of RW compression of plasmas in the strong-drive regime, it is now clear that this technique is robust and quite generally applicable to single component plasmas. It is particularly convenient for compression of positron-mass particles, where cooling can be accomplished under UHV conditions by cyclotron radiation. One outstanding issue is the density limit for this technique and, at present, this is an open question.

In the area of beam formation by pulsed extraction from the center of a single-component plasma, many of the questions have been answered, but other challenges remain. They include establishing beam extraction from cryogenic plasmas and demonstrating the ability to extract such beams from the magnetic field for further tailoring or use with electrostatic manipulation techniques. Finally, a number of the technical requirements for a practical, multicell positron trap have been established. One might envision construction of such a trap for $\sim 10^{12}$ particles in the next few years.

ACKNOWLEDGMENTS

We wish to acknowledge the collaboration of T. M. O'Neil and M. W. Anderson in developing a theoretical model of RW compression in the strong-drive regime and the expert technical assistance of E. A. Jerzewski. This work was supported by the U. S. National Science Foundation, grant PHY 07-13958.

REFERENCES

1. C. M. Surko and R. G. Greaves, *Phys. Plasmas* **11**, 2333-2348 (2004).
2. M. Amoretti, C. Amsler, G. Bonomi, A. Bouchta, P. Bowe, C. Carraro, C. L. Cesar, M. Charlton, M. Collier, M. Doser, V. Filippini, K. Fine, A. Fontana, M. Fujiwara, R. Funakoshi, P. Genova, J. Hangst, R. Hayano, M. Holzscheiter, L. Jorgensen, V. Lagomarsino, R. Landua, D. Lindelof, E. L. Rizzini, M. Macri, N. Madsen, G. Munuzio, M. Marchesotti, P. Montagna, H. Pruys, C. Regenfus, P. Riedler, J. Rochet, A. Rotondi, G. Rouleau, G. Testera, A. Variola, T. Watson, and D. VanderWerf, *Nature* **419**, 456-459 (2002).
3. G. Gabrielse, N. Bowden, P. Oxley, A. Speck, C. Storry, J. Tan, M. Wessels, D. Grzonka, W. Oelert, G. Schepers, T. Sefzick, J. Walz, H. Pittner, T. Hansch, and E. Hessels, *Phys. Rev. Lett.* **89**, 213401 1-4 (2002).
4. G. Gabrielse, N. Bowden, P. Oxley, A. Speck, C. Storry, J. Tan, M. Wessels, D. Grzonka, W. Oelert, G. Schepers, T. Sefzick, J. Walz, H. Pittner, T. Hansch, and E. Hessels, *Phys. Rev. Lett.* **89**, 233401 1-5 (2002).
5. J. Ellis, *Nature* **424**, 631-634 (2003).
6. R. G. Greaves and C. M. Surko, *Phys. Plasmas* **4**, 1528-1543 (1997).
7. S. J. Gilbert, D. H. E. Dubin, R. G. Greaves, and C. M. Surko, *Phys. Plasmas* **8**, 4982-4994 (2001).
8. T. S. Pederson, A. H. Boozer, W. Dorland, J. P. Kremer, and R. Schmitt, *J. Phys. B: At. Mol. Opt.* **36**, 1029-1039 (2003).
9. M. Charlton and J. W. Humberston, *Positron Physics* (Cambridge Univ. Press, Cambridge, U. K., 2001).
10. C. M. Surko, *New Directions in Antimatter Chemistry and Physics,* C. M. Surko and F. A. Gianturco, eds. (Kluwer Scientific Publishers, the Netherlands, 2001).
11. K. Iwata, R. G. Greaves, and C. M. Surko, *Can. J. Phys.* **51**, 407-410 (1996).
12. N. Guessoum, P. Jean, and W. Gillard, *Appl. Surf. Sci.* **252**, 3352 - 3361 (2006).
13. J. N. Sun, D. W. Gidley, Y. F. Hu, W. E. Frieze, and S. Yang, *Mat. Res. Soc. Symp. Proceedings* **726**, Q10.5 (2002).
14. B. Barbiellini, M. Weber, K. Lynn, P. Sterne, and A. Denison, *Mat. Res. Soc. Proceedings* **704** (2002).
15. C. Hugenschmidt, K. Schreckenbach, M. Stadlbauer, and B. Straßer, *Appl. Surf. Sci.* **252**, 3098-3105 (2006).
16. R. Krause-Rehberg, S. Sachert, G. Brauer, A. Rogov, and K. Noack, *Appl. Surf. Sci.* **252**, 3106-3110 (2006).
17. H. M. Chen, Y. C. Jean, C. D. Jonah, S. Chemerisov, A. F. Wagner, D. M. Schrader, and A. W. Hunt, *Appl. Surf. Sci.* **252**, 3159-3165 (2006).
18. A. G. Hathaway, M. Skalsey, W. E. Frieze, R. S. Vallery, and D. W. Gidley, *Nucl. Instrum. and Meth. in Phys. Res. A* **579**, 538-541 (2007).
19. D. B. Cassidy, S. H. M. Deng, R. G. Greaves, and A. P. Mills, Jr., *Rev. Sci. Instrum.* **77**, 073106-08 (2006).
20. D. B. Cassidy and A. P. Mills, Jr., *Nature* **449**, 195-197 (2007).
21. P. M. Platzman and A. P. Mills, Jr., *Phys. Rev. B* **49**, 454-458 (1994).
22. A. P. Mills, Jr., *Nucl. Instrum. Methods B* **192**, 107-116 (2002).
23. T. S. Pedersen, A. H. Boozer, J. P. Kremer, and R. G. Lefrancois, *Fusion Sci. and Tech.* **46**, 200-208 (2003).
24. J. R. Danielson and C. M. Surko, *Phys. Rev. Lett.* **95**, 035001-035004 (2005).
25. J. R. Danielson, T. R. Weber, and C. M. Surko, *Appl. Phys. Lett.* **90**, 081501 1-3 (2007).
26. T. R. Weber, J. R. Danielson, and C. M. Surko, *Phys. Plasmas* **15**, 012106 1-10 (2008).
27. C. M. Surko and R. G. Greaves, *Rad. Chem. and Phys.* **68**, 419 (2003).
28. J. R. Danielson, T. R. Weber, and C. M. Surko, *Phys. Plasmas* **13**, 123502 1-10 (2006).
29. J. R. Danielson and C. M. Surko, *Phys. Plasmas* **13**, 055706 1-10 (2006).
30. D. L. Eggleston, C. F. Driscoll, B. R. Beck, A. W. Hyatt, and J. H. Malmberg, *Phys. Fluids B* **4**, 3432-3439 (1992).
31. E. M. Hollmann, F. Anderegg, and C. F. Driscoll, *Phys. Plasmas* **7**, 2776-2789 (2000).
32. X. P. Huang, J. J. Bollinger, T. B. Mitchell, and W. M. Itano, *Phys. Rev. Lett.* **80**, 73-76 (1998).
33. R. G. Greaves and C. M. Surko, *Phys. Rev. Lett.* **85**, 1883-1886 (2000).
34. L. V. Jorgensen, M. Amoretti, G. Bonomi, P. D. Bowe, C. Canali, C. Carraro, C. L. Cesar, M. Charlton, and M. Doser, *Phys. Rev. Lett.* **95**, 025002 1-4 (2005).
35. J. R. Danielson, C. M. Surko, and T. M. O'Neil, *Phys. Rev. Lett.* **99**, 135005 1-4 (2007).